Magnetic Resonance Imaging 60 (2019) 38–43

Contents lists available at ScienceDirect

Magnetic Resonance Imaging

journal homepage: www.elsevier.com/locate/mri

Original contribution

Golden-angle radial sparse parallel (GRASP) MRI in clinical routine detection of pituitary microadenomas: First experience and feasibility

Nicolin Hainc[a,b,*], Christoph Stippich[a,b], Julia Reinhardt[a,b], Bram Stieltjes[c], Maria Blatow[a,b], Luigi Mariani[d], Andrea Bink[a,b]

[a] Department of Neuroradiology, Clinical Neuroscience Center, University Hospital Zurich, University of Zurich, Zurich, Switzerland
[b] Division of Diagnostic and Interventional Neuroradiology, Department of Radiology, University Hospital Basel, University of Basel, Basel, Switzerland
[c] Department of Radiology, University Hospital Basel, University of Basel, Basel, Switzerland
[d] Department of Neurosurgery, University Hospital Basel, University of Basel, Basel, Switzerland

ARTICLE INFO

Keywords:
Magnetic resonance imaging
Brain
Neoplasms
Pituitary MRI

ABSTRACT

Background and purpose

To demonstrate the clinical feasibility of a novel MRI pulse sequence, Golden-angle radial sparse parallel MRI (GRASP) through comparison to the current imaging technique, dynamic T1- weighted contrast enhanced (DCE) imaging in terms of image quality and lesion depiction in the detection of microlesions (microadenomas and cysts) of the pituitary gland.

Materials and methods: 16 patients (11 microadenomas, 5 cysts) underwent two MRI examinations (Siemens 1.5T and 3T) on separate dates, one using standard DCE (temporal resolution 30 s) and the other using GRASP (temporal resolution of 4.4 s). Two neuroradiologists separately recorded measures of image quality (Scale 1–5, 5 = best), lesion size and contrast arrival times in terms of first and best lesion conspicuity.

Results: In qualitiative analysis there were no significant differences in terms of average visual image sharpness (DCE 3.9 ± 0.9, GRASP 3.9 ± 0.9) or visual contrast scores (DCE 4.1 ± 1.2, GRASP 4.4 ± 0.8). Pearson's correlation coefficients for interreader lesion measurements (width and height, mm) ranged from substantial to almost perfect agreement (r = 0.73 to 0.88). Analysis of contrast arrival times revealed an average lesion first-conspicuity time of 60.7 ± 16.7 s for DCE compared to 50.2 ± 10.3 s for GRASP with a difference of 10.5 ± 16.2 s (p = 0.023).

Conclusion: Depiction of pituitary microlesions is feasible with GRASP, which has the potential to increase sensitivity through higher temporal resolutions combined with isotropic acquisition allowing for multi-planar reconstructions; this remains to be proven in larger cohorts.

1. Introduction

The clinical syndromes induced by pituitary adenomas result in a marked reduction in quality of life for the patient; the estimated prevalence of these lesions in the population ranges from 14 to 23% [1]. Morphologically, pituitary adenomas are classified into microadenomas (< 1 cm) or macroadenomas (≥1 cm) based on size, yet the lesions can be further classified based on hormonal activity. Hormonally active adenomas usually present with syndromes according to the hormonal imbalance they induce while hormonally inactive adenomas tend to grow to a larger size before being discovered and present with syndromes based on visual disturbances either by affecting the optic nerve or invading the cavernous sinus. The diagnosis of pituitary adenomas is based on clinical assessment, imaging and endocrinological work up.

While macroadenomas lead to an expansion and deformation of the gland which can be seen on various MRI pulse sequences, microadenomas are often very small and present an imaging challenge. The. unique and predictable enhancement of the pituitary gland results from its unique vascular supply. While the neurohypophysis is supplied directly by the inferior hypophyseal arteries, the adenohypophysis is supplied indirectly by the superior hypophyseal arteries through the portal venous system of the pituitary, resulting in a slower, characteristic pattern of enhancement [2,3]: posterior lobe, stalk, median eminence, pars distalis, then radially out towards the borders of the gland.

Abbreviations: MRI, Magnetic resonance imaging; GRASP, Golden angle radial sparse parallel; DCE, Dynamic contrast enhanced; T, Tesla; SNR, Signal to noise ratio; RIS, Radiological information system

* Corresponding author at: Department of Neuroradiology, University Hospital Zurich, Frauenklinikstrasse 10, 8091, Zurich, Switzerland.
E-mail address: nicolin.hainc@usz.ch (N. Hainc).

https://doi.org/10.1016/j.mri.2019.03.015
Received 23 January 2019; Received in revised form 7 March 2019; Accepted 19 March 2019

A dynamic contrast enhanced (DCE), multi-slice T1 weighted MRI pulse sequence is part of the current imaging standard protocol along with T2-weighed imaging for the detection of microadenomas [4], yet smaller lesions between individual slices can be overlooked. An attempt to increase sensitivity through the addition of sagittal dynamic contrast enhanced imaging [5] directly after coronal imaging resulted in limited success; reported sensitivity was increased from 61.1% to 88.9%, yet the practice was not widely adopted, mainly due to the fact that it required administration of double or triple dose contrast agent.

A recent advancement in MR-Imaging through a pulse sequence known as golden angle radial sparse parallel (GRASP) proposes to improve dynamic pituitary imaging – temporal resolutions of up to 2.5 s per image [2] combined with 3D submillimeter isotropic acquisitions allow for very high resolution studies combined with the increased sensitivity of multiplanar imaging in a single contrast administration. GRASP is a gradient echo pulse sequence employing rapid acquisition and reconstruction techniques known as radial "stack-of-stars" k-space sampling [6], golden-angle ordering [7], compressed sensing, parallel imaging [8] allowing for a continuous 3D data acquisition of first-pass contrast enhancement; its feasibility has already been established in the prostate [9], breast, head and neck, and liver- even proving to be robust to motion during free breathing [10]. Detailed information on the sequence can be found in the work by Feng et al. [10]. The continuously acquired data can then be postprocessed into user defined timeframes in a reciprocal trade off with signal-to-noise ratio (SNR) with higher temporal resolutions resulting in lower SNR. The high temporal resolution allows for the creation of high-resolution signal time curves already shown to allow for effortless differentiation of cystic pituitary lesions from microadenomas [2].

The characteristic contrast enhancement pattern of the pituitary combined with the distinct enhancement of microadenomas make GRASP an ideal candidate for dynamic contrast enhanced pituitary imaging. Consequently, the aim of this study was to compare GRASP qualitatively to the current imaging standard of pituitary microadenomas, DCE, to demonstrate its feasibility in clinical routine.

2. Materials and methods

2.1. Patients

This retrospective study was approved by the institutional review board before proceeding and all methods were carried out in accordance with the approved guidelines. Written informed consent was established. A RIS (radiological information system) based search for patients imaged with our GRASP-based pituitary microadenoma protocol was performed between January 2014 and September 2017. Second, the imaging history of each patient was analysed to establish that the standard DCE had also been performed at another timepoint, either before or after the GRASP study; only patients with both GRASP and DCE studies were included with an average of 15.9 ± 10.1 months between examinations. 16 patients were included in the study: 11 microadenomas (correlated with endocrinological findings resulting in 6 prolactinomas, 1 adrenocorticotropic (ACTH)-secreting microadenoma, 1 human growth hormone (HGH)-secreting microadenoma, 3 endocrine-inactive microadenomas), 1 mixed lesion (components of a microadenoma and a cyst, no abnormal endocrine findings), and 4 cystic microlesions, most likely rathke cleft cysts (no abnormal endocrine findings). There were no changes in therapy between the two scans for all microadenoma patients.

2.2. MR imaging

The GRASP imaging protocol was performed on two MRI scanners, Siemens (Siemens Healthineers, Erlangen, Germany) Skyra 3T and Skyra FIT 3T with following Parameters: TR/TE 4.4/2.1 ms, flip angle 12°, slice thickness 1 mm, 112 slices, FOV 256 × 256, matrix 256 × 256; 610 Spokes, acquisition time 276 s. Bandwidth 400 Hz/Px. Temporal resolution 4.4 s (see Image Analysis and Processing for details on temporal resolution).

The DCE imaging protocol was performed on multiple scanners using dedicated, dynamic T1-weighted pulse sequences optimized for the pituitary gland with following parameters: GE (General Electric, Chicago, Illinois) Discovery 750 3T: TR/TE 438/15 ms, flip angle 7°, slice thickness 3 mm, 9 slices, FOV 180 × 180, matrix 192 × 224, bandwidth 75 Hz/Px. Siemens (Siemens Healthineers, Erlangen, Germany) Skyra 3T: TR/TE 550/9 ms, flip angle 70°, slice thickness 3 mm, 11 slices, FOV 180 × 180, matrix 240 × 320, bandwidth 260 Hz/Px. Siemens Espree 1.5T: TR/TE 556/17 ms, flip angle 141°, slice thickness 3 mm, 12 slices, FOV 140 × 140, matrix 205 × 256, bandwidth 130 Hz/Px. Siemens Avanto FIT 1.5T: TR/TE 320/8 ms, flip angle 141°, slice thickness 3 mm, 7 slices, FOV 163 × 200, matrix 146 × 256, bandwidth 195 Hz/Px. Siemens Symphony 1.5T: TR/TE

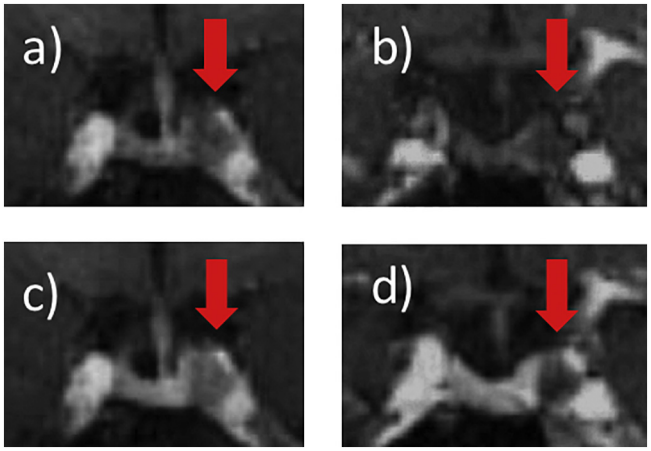

Fig. 1. Timepoints of first lesion conspicuity (top row; GRASP left, DCE right) and best lesion contrast (bottom row; GRASP left, DCE right). For the GRASP images, the internal carotid artery and cavernous sinus appear to create a near 360° contrast around the pituitary microadenoma (a). On further inspection, at a later timepoint (c), a thin strip of enhancing pituitary parenchyma can be seen at the superior and supero-medial aspects of the microadenoma, justifying the later timepoint as "time of best contrast". DCE images at first lesion conspicuity (b) and best contrast (d).

Table 1
Summary of average time of first lesion conspicuity and best lesion contrast with differences and *p* values listed on the right.

Time measurement	Reader average (s)		Difference (s)	p Value
	GRASP	DCE		
First conspicuous	50.2 ± 10.3	60.7 ± 16.7	10.5 ± 16.2	p = 0.023
Best contrast	77.4 ± 23.6	91.9 ± 39.5	14.5 ± 48.9	$p > 0.05$

Table 2
Statistical analysis of lesion measurements comparing GRASP and DCE. Interreader correlation (comparing both reader's measured lesion height and width for GRASP and DCE) in terms of Pearson's correlation coefficient (above). Intrareader comparison (comparing a reader's measured lesion height and width for GRASP and DCE) in terms of Bland-Altman plots and linear regression of the plots (below).

Interreader correlation	Height	Width
GRASP, R1 vs R2	0.88	0.756
DCE, R1 vs R2	0.8	0.731
Intrareader Bland-Altman, L. Regression		
R1, GRASP vs DCE	$t > 0.05$	$t > 0.05$
R2, GRASP vs DCE	$t > 0.05$	$t > 0.05$

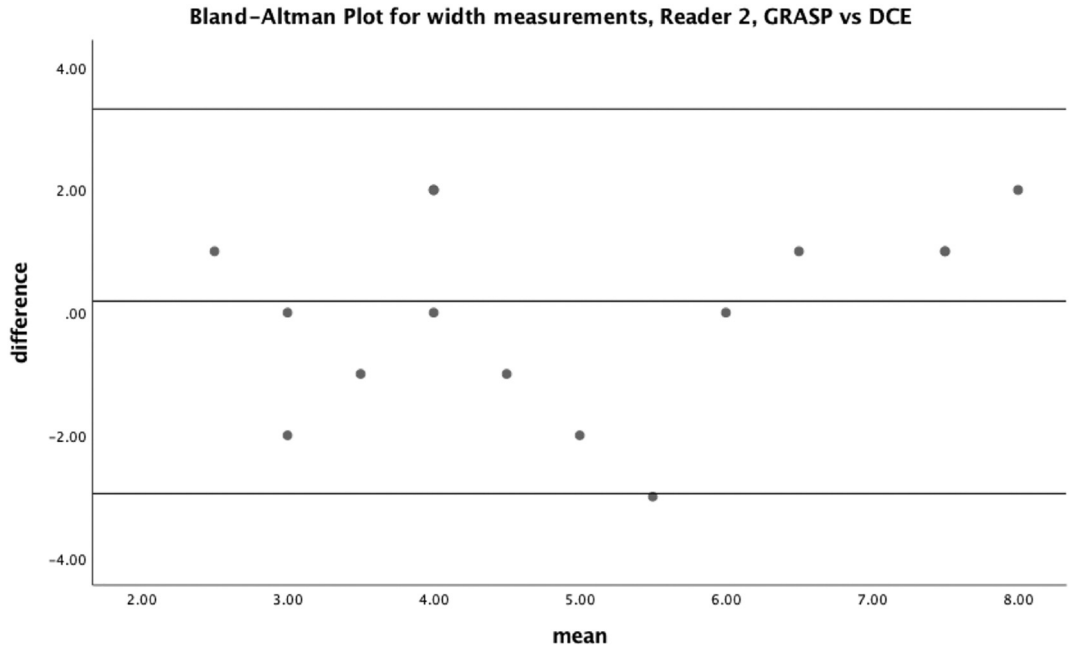

Fig. 2. Example of a Bland-Altman plot for width measurements comparing GRASP and DCE; difference of the lesion measurements (DCE-GRASP) along the Y axis with confidence intervals at ± (SD x 1.96), mean of the lesion measurements (DCE and GRASP) along the X axis. Overlapping values resulted in the appearance of less data points (13 data points for 16 data sets).

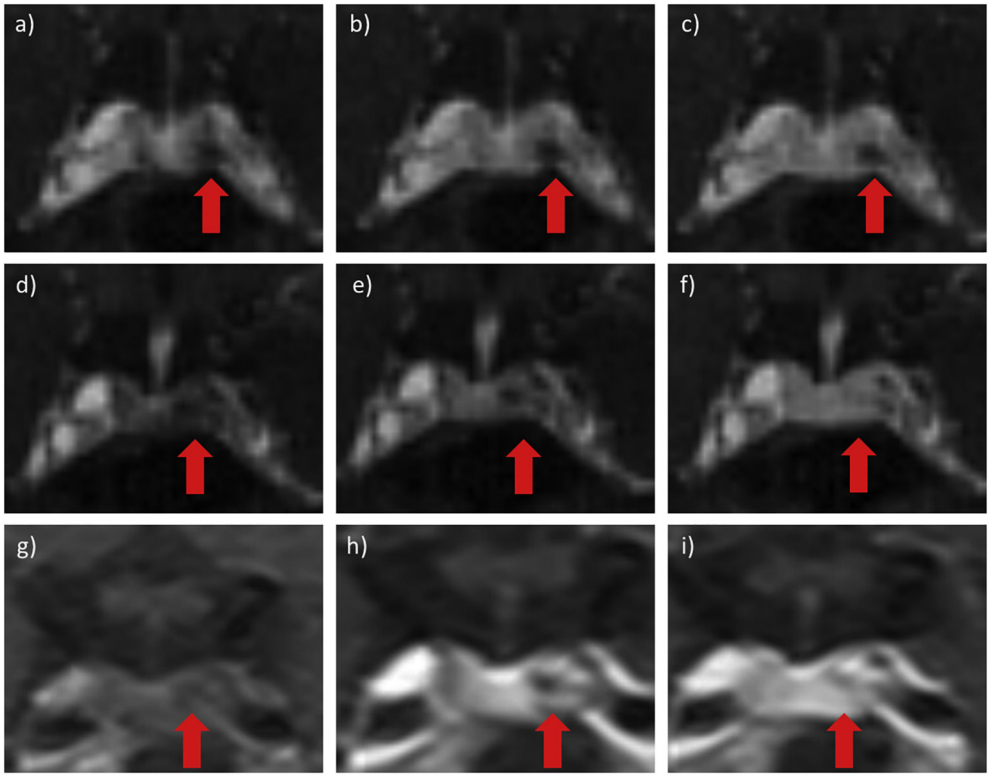

Fig. 3. Added value of GRASP: The cystic and solid components of the lesion can only be appreciated using GRASP. Top row: Time series at the level of the cystic aspect of the lesion, from an earlier timepoint (a) through to a later timepoint (c) showing no enhancement throughout. Middle row: solid aspect of the lesion showing delayed enhancement from an earlier timepoint (d) through to a later timepoint (f). Confidence is further increased using region of interest (ROI) analysis of the two components (see chart on the right). Bottom row: DCE images from an earlier timepoint (g) through to a later timepoint (i), through the only slice depicting the lesion, showing a delayed enhancement and therefore a diagnosis of microadenoma.

320/9 ms, flip angle 141°, slice thickness 3 mm, 7 slices, FOV 159 × 200, matrix 143 × 320, bandwidth 256 Hz/Px. Temporal resolution for all MRI scanners was 30 s.

2.3. Image analysis and processing

Two readers AB and NH with 13 and 2 years of experience in neuroradiology blindly evaluated the randomly assorted GRASP and DCE imaging studies independently (6 sessions of 5–6 imaging studies per session). The acquired data from the GRASP scans were exported and reconstructed off-line by using a C++ implementation of the GRASP algorithm [10], creating a total of 43 timeframes: the first 40 timeframes were reconstructed for a temporal resolution of 4.4 s (13 spokes per timeframe), the last 3 timeframes (at the end of the examination) consisting of timeframes of 16 s, 28 s, and 28 s respectively. Reconstructed images were sent to the PACS and analysed using

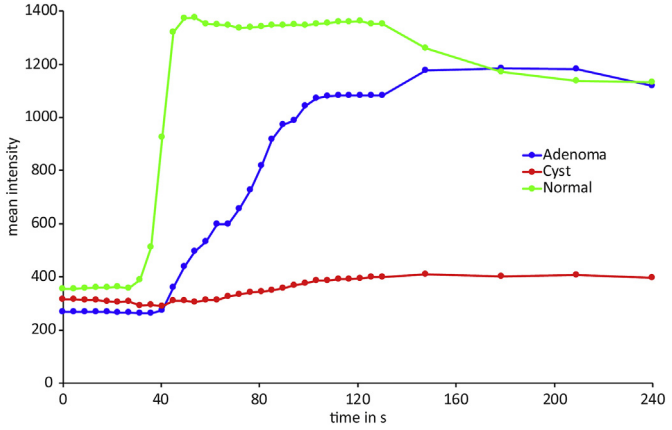

Fig. 4. Signal-time curves of regions of interest (ROIs) in the solid enhancing aspect of the lesion (blue), cystic non-enhancing aspect (red), and normal-appearing parenchyma on the opposite side of the gland (green). (For interpretation of the references to colour in this figure legend, the reader is referred to the web version of this article.)

syngo.via (Siemens Healthineers, Erlangen, Germany, Version VB20A) Software with the MR Basic workflow. DCE imaging studies were viewed in the picture archiving and communication system (Centricity PACS, GE Healthcare, Chicago, Illinois).

To assess image quality readers rated each sequence subjectively (Scale 1–5, 5 = best) in terms of image sharpness (how pixelated the pituitary gland and lesion appeared). Then readers were instructed to assess the dynamic images beginning with the coronal slices to assess following features: 1) microadenoma or cystic lesion, 2) confidence in the given diagnosis. Lesion dimensions were measured in the X and Y plane on coronal images.

Second, readers were instructed to indicate the time they subjectively found the lesion to be first conspicuous and the time they found the lesion to be best contrasted to the pituitary gland (Fig. 1). First conspicuous was defined by the timepoint that the reader could first indicate that a lesion was present. Best contrast was defined by the first timepoint in which contrast enhancement could be seen 360° around the lesion on the coronal slice with the largest lesion diameter. Subjective visual contrast (1–5 scale, 5 = best) was indicated for each of the aforementioned timepoints.

2.4. Statistical analysis

Statistical analysis was performed using IBM SPSS software (IBM Corp. IBM SPSS Statistics, Version 25.0. Armonk, NY). The subjective image scores were compared between DCE and GRASP using the paired Wilcoxon test. The significance level was set to $p < 0.05$. For inter-reader lesion measurements (GRASP vs GRASP, DCE vs DCE), pearson's correlation coefficient was used and rated as follows: 0–0.20, slight agreement; 0.21–0.40, fair agreement; 0.41–0.60, moderate agreement; 0.61–0.80, substantial agreement; 0.81–1.00, almost perfect agreement [11]. For intrareader measurements between GRASP and DCE, Bland-Altman analysis and linear regression of the Bland-Altman plots was performed. Times of first lesion conspicuity and best lesion contrast between DCE and GRASP were compared using the paired Wilcoxon test. The significance level was set to $p < 0.05$.

3. Results

3.1. Qualitative analysis

In qualitative analysis there were no significant differences in terms of average visual image sharpness (DCE 3.9 ± 0.9, GRASP 3.9 ± 0.9), confidence in diagnosis (DCE 4.3 ± 1.4, GRASP 4.3 ± 0.75,) or visual contrast scores (first conspicuous DCE 3.7 ± 0.9, GRASP 3.5 ± 0.9, best contrast DCE 4.1 ± 1.2, GRASP 4.4 ± 0.8,) between the two imaging techniques.

3.2. Quantitative analysis

Analysis of contrast arrival times revealed an average lesion first-conspicuity time of 60.7 ± 16.7 s for DCE compared to 50.2 ± 10.3 s for GRASP with a significant difference of 10.5 ± 16.2 s ($p = 0.023$) (Table 1). Lesion best-contrast was 91.9 ± 39.5 s for DCE compared to 77.4 ± 23.6 s for GRASP. Pearson's correlation coefficients for inter-reader lesion measurements (GRASP vs GRASP, DCE vs DCE, width and height, mm) ranged from substantial to almost perfect agreement ($r = 0.73$ to 0.88) (Table 2). For intrareader measurements (GRASP vs DCE, width and height, mm) Bland-Altman analysis (Fig. 2) with linear regression revealed no significant proportional bias (all t scores > 0.05).

4. Discussion

To our knowledge, the temporal resolution of 4.4 s in the GRASP sequence is the highest published resolution for the assessment of pituitary microadenomas to date, with 10 s being the previous best [12–15]. Compared to DCE in our study, which has a temporal resolution of 30 s, GRASP allows visualization of pituitary lesion enhancement at an earlier timepoint demonstrating its potential to

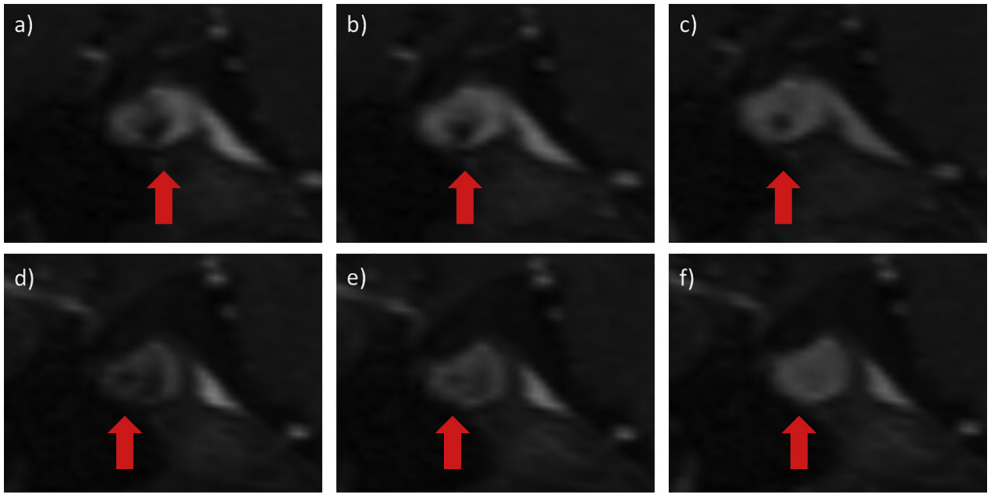

Fig. 5. Added value of GRASP: sagittal plane. Top row: Time series at the level of the cystic aspect of the lesion, from an earlier timepoint (a) through to a later timepoint (c) showing no enhancement throughout. Lower row: solid aspect of the lesion showing delayed enhancement from an earlier timepoint (d) through to a later timepoint (f).

characterize lesions with a higher accuracy. As a further testament to the clinical feasibility of GRASP, no significant differences were found on visual comparison of the two imaging techniques, even though the in-plane resolution for the isotropic GRASP voxels was slightly less than the anisotropic DCE voxels. Readers noted no significant artefacts due to magnetic susceptibility interfaces which can be an issue when imaging near the skull base [16], especially with gradient-echo sequences such as GRASP. Moreover, the thinner slice thickness in GRASP results in less volume averaging, theoretically increasing sensitivity of very small microadenomas. Additionally, the isotropic voxels in GRASP allow for sagittal reconstruction of the first-pass dynamic contrast enhanced study, a method already shown to increase sensitivity in microadenoma detection [5] currently requiring, however, dedicated sagittal slices and a second administration of double or even triple dose contrast. Again, the advantage of GRASP is clear, all planes can be assessed using only a single dose of contrast.

A recent GRASP based dynamic pituitary study with a reconstructed temporal resolution of 20 s describes full enhancement of the gland at 90 s [2], and while most pituitary microadenomas enhance with a relative delay compared to the adenohypophysis, lesions exist with a relative earlier contrast enhancement, most likely due to a direct arterial blood supply [17]. Our results could be extrapolated to lesions of this nature as well - detection of these lesions may warrant a higher temporal resolution in the timeframe before the anterior pituitary begins its characteristic enhancement.

The reconstructed GRASP data opened in the MR Basic workflow in syngo.via software also allows for high-resolution signal-time curves for regions of interest to be created. One study by Rossi et al. [2] using GRASP has shown that cysts can be differentiated from microadenomas with relative ease; cysts demonstrated a flat signal time curve, microadenomas demonstrated a steadily increasing enhancement with a peak at 90 s and a relative plateau. In our study, in one case, both readers individually noted that GRASP combined with the signal-time curve helped in the characterization of a microlesion which appeared to have both solid and cystic components (Fig. 3). Here, the signal-time curve (Fig. 4) added to reader confidence in characterizing the lesion, displaying both a flat curve (cystic component) and a slower yet steadily increasing curve (solid component) when compared to the normal appearing contralateral side of the gland. On DCE, the lesion appeared to consist of solid components only, most likely due to the volume averaging effects of the thicker slices. Effectively, DCE leads to a larger microadenoma measurement, potentially resulting in different management were this to be an incidental finding [18]. The ability to utilize the same dynamic contrast series in the sagittal plane provided yet another benefit of the GRASP sequence, as both aspects of the solid and cystic lesion could be visualized (Fig. 5). GRASP's high-resolution signal-time curves and potential application in pharmacokinetic analysis [19] create accurate, quantitative biomarkers, extracting further tumor information from imaging studies thus representing a further element in radiology's pursuit of radiomics [20]. It is conceivable that, through studies with larger cohorts of microadenomas correlated with endocrine findings or biopsies, unique high-resolution signal-time curves for individual microadenoma subtypes could be established.

The small cohort size is an obvious limitation of our study. Ideally, patients would have been scanned using both techniques on the same day for optimal comparison purposes. This practice, however, does not represent clinical routine, and while patients were scanned on separate dates with an average of 15.9 ± 10.1 months between scans, only those with unchanged lesion size on follow up were included. Furthermore, there was no change in therapy in any of the patients between the two scans. While DCE was performed on different MRI scanners of different field strengths (1.5T, 3T), subgroup analysis of differing magnetic field strengths was deemed not possible due to small cohort size. A signal-to-noise (SNR) comparison is also beyond the scope of our feasibility study, as the SNR in GRASP is directly related to the user defined server-reconstruction timeframes. All of our pituitary studies were performed using an identical high temporal resolution, low SNR timeframe. A comparison of differing reconstructions of raw GRASP data is warranted to determine optimal timeframes for pituitary imaging. Finally, while endocrine abnormalities were correlated with the microlesions, biopsy is unquestionably the gold standard in lesion characterization.

Many more applications of the GRASP sequence must be tested for pituitary imaging, for example in the assessment of residual/recurrent adenoma and differentiation of scar tissue within the sella in the postoperative setting. Larger cohorts are required for further validation and investigation of unique signal-time curves for microadenoma subtypes. Our work represents an initial step in proving the clinical feasibility of the GRASP sequence, even highlighting the additional information it provides, and hints at future applications such as radiomics.

5. Conclusion

To conclude, while the in-plane resolution for the isotropic GRASP voxels was slightly less than the anisotropic DCE voxels, no significant difference in visual assessment was found on GRASP images, demonstrating its feasibility in detecting microlesions of the pituitary gland. The advantage of higher temporal resolutions and the benefit of sagittal reconstructions with GRASP might offer better diagnostic yield than DCE which is to be proved in larger cohorts.

Conflict of interest

We declare that we have no conflict of interest.

Funding

This research did not receive any specific grant from funding agencies in the public, commercial, or not-for-profit sectors.

Appendix A. Supplementary data

Supplementary data to this article can be found online at https://doi.org/10.1016/j.mri.2019.03.015.

References

[1] Ezzat S, Asa SL, Couldwell WT, Barr CE, Dodge WE, Vance ML, et al. The prevalence of pituitary adenomas: a systematic review. Cancer 2004;101:613–9. https://doi.org/10.1002/cncr.20412.
[2] Rossi Espagnet MC, Bangiyev L, Haber M, Block KT, Babb J, Ruggiero V, et al. High-resolution DCE-MRI of the pituitary gland using radial k-space acquisition with compressed sensing reconstruction. AJNR Am J Neuroradiol 2015;36:1444–9. https://doi.org/10.3174/ajnr.A4324.
[3] Tien RD. Sequence of enhancement of various portions of the pituitary gland on gadolinium-enhanced MR images: correlation with regional blood supply. AJR Am J Roentgenol 1992;158:651–4. https://doi.org/10.2214/ajr.158.3.1739013.
[4] Rand T, Lippitz P, Kink E, Huber H, Schneider B, Imhof H, et al. Evaluation of pituitary microadenomas with dynamic MR imaging. Eur J Radiol 2002;41:131–5.
[5] Gao R, Isoda H, Tanaka T, Inagawa S, Takeda H, Takehara Y, et al. Dynamic gadolinium-enhanced MR imaging of pituitary adenomas: usefulness of sequential sagittal and coronal plane images. Eur J Radiol 2001;39:139–46.
[6] Chandarana H, Block TK, Rosenkrantz AB, Lim RP, Kim D, Mossa DJ, et al. Free-breathing radial 3D fat-suppressed T1-weighted gradient echo sequence: a viable alternative for contrast-enhanced liver imaging in patients unable to suspend respiration. Invest Radiol 2011;46:648–53. https://doi.org/10.1097/RLI.0b013e31821eea45.
[7] Winkelmann S, Schaeffter T, Koehler T, Eggers H, Doessel O. An optimal radial profile order based on the Golden ratio for time-resolved MRI. IEEE Trans Med Imaging 2007;26:68–76. https://doi.org/10.1109/TMI.2006.885337.
[8] Chandarana H, Feng L, Block TK, Rosenkrantz AB, Lim RP, Babb JS, et al. Free-breathing contrast-enhanced multiphase MRI of the liver using a combination of compressed sensing, parallel imaging, and golden-angle radial sampling. Invest Radiol 2013;48:10–6. https://doi.org/10.1097/RLI.0b013e318271869c.
[9] Rosenkrantz AB, Geppert C, Grimm R, Block TK, Glielmi C, Feng L, et al. Dynamic contrast-enhanced MRI of the prostate with high spatiotemporal resolution using compressed sensing, parallel imaging, and continuous golden-angle radial sampling: preliminary experience. J Magn Reson Imaging 2015;41:1365–73. https://doi.org/

10.1002/jmri.24661.
[10] Feng L, Grimm R, Block KT, Chandarana H, Kim S, Xu J, et al. Golden-angle radial sparse parallel MRI: combination of compressed sensing, parallel imaging, and golden-angle radial sampling for fast and flexible dynamic volumetric MRI. Magn Reson Med 2014;72:707–17. https://doi.org/10.1002/mrm.24980.
[11] Landis JR, Koch GG. The measurement of observer agreement for categorical data. Biometrics 1977;33:159–74.
[12] Kucharczyk W, Bishop JE, Plewes DB, Keller MA, George S. Detection of pituitary microadenomas: comparison of dynamic keyhole fast spin-echo, unenhanced, and conventional contrast-enhanced MR imaging. AJR Am J Roentgenol 1994;163:671–9. https://doi.org/10.2214/ajr.163.3.8079866.
[13] Sakamoto Y, Takahashi M, Korogi Y, Bussaka H, Ushio Y. Normal and abnormal pituitary glands: gadopentetate dimeglumine-enhanced MR imaging. Radiology 1991;178:441–5. https://doi.org/10.1148/radiology.178.2.1987606.
[14] Agati R, Maffei M, Bacci A, Cevolani D, Battaglia S, Leonardi M. 3 T MR assessment of pituitary microadenomas: a report of six cases. Riv Neuroradiol 2004;17:890–5. https://doi.org/10.1177/197140090401700618.
[15] Chaudhary V, Bano S. Imaging of the pituitary: recent advances. Indian J Endocrinol Metab 2011;15:S216–23. https://doi.org/10.4103/2230-8210.84871.
[16] Elster AD. Sellar susceptibility artifacts: theory and implications. AJNR Am J Neuroradiol 1993;14:129–36.
[17] Yuh WT, Fisher DJ, Nguyen HD, Tali ET, Gao F, Simonson TM, et al. Sequential MR enhancement pattern in normal pituitary gland and in pituitary adenoma. AJNR Am J Neuroradiol 1994;15:101–8.
[18] Hoang JK, Hoffman AR, González RG, Wintermark M, Glenn BJ, Pandharipande PV, et al. Management of Incidental Pituitary Findings on CT, MRI, and 18F-fluorodeoxyglucose PET: a white paper of the ACR incidental findings committee. J Am Coll Radiol JACR 2018. https://doi.org/10.1016/j.jacr.2018.03.037.
[19] Zhai J, Zheng W, Zhang Q, Wu J, Zhang X. Pharmacokinetic analysis for the differentiation of pituitary microadenoma subtypes through dynamic contrast-enhanced magnetic resonance imaging. Oncol Lett 2019. https://doi.org/10.3892/ol.2019.10083.
[20] Gillies RJ, Kinahan PE, Hricak H. Radiomics: images are more than pictures, they are data. Radiology 2016;278:563–77. https://doi.org/10.1148/radiol.2015151169.